Icarus 270 (2016) 197–210

Contents lists available at ScienceDirect

Icarus

journal homepage: www.journals.elsevier.com/icarus

Variations in Titan's dune orientations as a result of orbital forcing

George D. McDonald [a,b,*], Alexander G. Hayes [b], Ryan C. Ewing [c], Juan M. Lora [d], Claire E. Newman [e], Tetsuya Tokano [f], Antoine Lucas [g], Alejandro Soto [h], Gang Chen [i]

[a] School of Earth and Atmospheric Sciences, Georgia Institute of Technology, Atlanta, GA 30308, USA
[b] Department of Astronomy, Cornell University, Ithaca, NY 14853, USA
[c] Department of Geology and Geophysics, Texas A&M University, College Station, TX 77840, USA
[d] Department of Earth, Planetary, and Space Sciences, University of California, Los Angeles, Los Angeles, CA 90095, USA
[e] Ashima Research, Pasadena, CA 91001, USA
[f] Institut für Geophysik und Meteorologie, Universität zu Köln, 50923 Köln, Germany
[g] AIM CEA-Saclay, Paris VII-Denis Diderot University, Paris 75013, France
[h] Southwest Research Institute, Boulder, CO 80032, USA
[i] Department of Earth and Atmospheric Sciences, Cornell University, Ithaca, NY 14853, USA

ARTICLE INFO

Article history:
Received 28 July 2015
Revised 31 October 2015
Accepted 29 November 2015
Available online 2 January 2016

Keywords:
Titan
Titan, surface
Titan, atmosphere
Atmospheres, dynamics

ABSTRACT

Wind-blown dunes are a record of the climatic history in Titan's equatorial region. Through modeling of the climatic conditions associated with Titan's historical orbital configurations (arising from apsidal precessions of Saturn's orbit), we present evidence that the orientations of the dunes are influenced by orbital forcing. Analysis of 3 Titan general circulation models (GCMs) in conjunction with a sediment transport model provides the first direct intercomparison of results from different Titan GCMs. We report variability in the dune orientations predicted for different orbital epochs of up to 70°. Although the response of the GCMs to orbital forcing varies, the orbital influence on the dune orientations is found to be significant across all models. Furthermore, there is near agreement among the two models run with surface topography, with 3 out of the 5 dune fields matching observation for the most recent orbital cycle. Through comparison with observations by Cassini, we find situations in which the observed dune orientations are in best agreement with those modeled for previous orbital configurations or combinations thereof, representing a larger portion of the cycle. We conclude that orbital forcing could be an important factor in governing the present-day dune orientations observed on Titan and should be considered when modeling dune evolution.

© 2015 Elsevier Inc. All rights reserved.

1. Introduction

Titan's equatorial region is dominated by dunes. These dunes are unique in the Solar System for both their extensive spatial coverage (Le Gall et al., 2011) and inferred organic composition (Barnes et al., 2008). The interaction of these bedforms with surface winds makes them especially valuable for reconstructing Titan's climate over a significant fraction of the surface. Information about Titan's near-surface winds is of utility both for understanding surface evolution (Lorenz et al., 2006; Tokano, 2010) and planning future exploration (Lorenz, 2008; Barnes et al., 2012).

Important information about the surface wind regime has been provided by studies of the morphologic characteristics of the dunes. Lorenz et al. (2006) indicated that the dunes are predominantly linear in nature, with such dunes typically associated with a dominant sediment transport direction along the axis of the dunes. Examination of the streamlining, or divergence and reconvergence, of these bedforms around topographic obstacles suggests exclusively eastward transport (Lorenz et al., 2006; Radebaugh et al., 2008; Lorenz and Radebaugh, 2009).

Despite the observational evidence for eastward transport which would be driven by westerlies (that is winds blowing from west to east), all general circulation models (GCMs) consistently predict easterly flow to dominate in the near-surface of Titan's equatorial region (Tokano, 2010; Lebonnois et al., 2014; Lora et al., 2015). This seeming contradiction between the direction of wind flow governing sediment transport, and that necessary for conserving atmospheric angular momentum has lead to numerous studies that attempt to reconcile the wind regime with eastward transport of dune material. Lorenz et al. (2006) suggested a tidally driven azimuthal component to the winds that could result in

* Corresponding author at: School of Earth and Atmospheric Sciences, Georgia Institute of Technology, Atlanta, GA 30308, USA.

http://dx.doi.org/10.1016/j.icarus.2015.11.036
0019-1035/© 2015 Elsevier Inc. All rights reserved.

eastward transport; however results from a GCM indicated that a complete rotation of the dominant equatorial wind due to tidal influences was not possible (Tokano, 2010). In Tokano (2010), GCM simulations produced fast westerly winds during equinoctial passage of the intertropical convergence zone. Despite their rare occurrence, these westerlies are faster than the easterlies and could in turn dominate sediment transport. Lucas et al. (2014) and Charnay et al. (2015) show that low latitude methane storms around equinox may produce strong westerlies by coupling the strongly superrotating winds aloft with the near-surface flow.

Despite the ability of these mechanisms to reconcile the dune propagation direction with the wind regime, they provide no constraints on the timescales necessary for equilibration of the dune orientations with changes to the wind regime. Investigation of the timescales necessary for the reorientation of Titan's dunes, based on estimates of crestline propagation rates, suggests timescales of order 50,000 years or greater (Lorenz, 2014; Ewing et al., 2015). Therefore, any of the previously indicated mechanisms which produce eastward dune propagation must consistently operate over a timescale greater than this. This finding also calls into question whether effects on the wind regime whose duty cycle is comparable to these reorientation timescales, specifically that of orbital precessions, could impact the dunes. The notion of dunes responding to an orbitally forced climate, even being in equilibrium with winds from a historical orbital epoch, has previously been indicated in terrestrial fieldwork where the largest dunes in the western Sahara Desert have been inferred to be oriented with respect to fast winds from the Last Glacial Maximum (Lancaster et al., 2002), and the dunes of the Gran Desierto Dune Field in Mexico have been dated to several different eras from the last glacial cycle (Beveridge et al., 2006). In the case of Titan, variations in Saturn's orbit affect Titan's climate (Lora et al., 2014), and this must be considered in studies of Titan's dunes. This forcing, which we refer to as Titan's Croll–Milankovitch cycles, has previously been tied to Titan's global-scale geomorphology in the suggestion of its governing Titan's polar lake distributions (Aharonson et al., 2009; Lora et al., 2014).

We present here the first investigation of the response of Titan's dunes to climatic variations driven by the Croll–Milankovitch forcing. This is accomplished through simulations of Titan's climate at historical and modern orbital configurations using three different GCMs, in conjunction with a sediment transport model. We find that regardless of which GCM is chosen, the orbital configuration affects the dune orientation, with as high as 70° variations in the dune orientation as a function of the orbital epoch. The inclusion of topography in the models is found to be important in generating eastward propagation of the dunes, and results in agreement with observation for three out of the five major dune fields for the two models run for the most recent orbital cycle. Although in certain situations a specific orbital epoch or combination thereof is found to be in best agreement with observation, there is no particular epoch that is universally in agreement with observation. We nonetheless demonstrate that the effect of orbital variations on the climate through changes in the solar insolation pattern is important for the prediction of dune orientations, and suggest that future modeling work which includes second order effects beyond the insolation changes may point to specific epochs or time periods that are in best agreement with the orientations observed today.

2. Methods

2.1. Orbital parameters

Variations in the perihelion passage, eccentricity and spin axis of Saturn's orbit affect Titan's climate (Lora et al., 2014). We note that the estimated obliquity of Titan itself with respect to Saturn is small at 0.3° (Stiles et al., 2008), not expected to vary significantly due to tidal locking, and is therefore ignored. Saturn's orbital parameters over the past 1 Myr (years always refers to Earth years unless otherwise specified) were solved for through integration of the SWIFT orbital position code (Levison and Duncan, 1994), along with calculation of obliquity changes through secular theory (Ward and Hamilton, 2004). The results suggest that Saturn's apsidal precessions and eccentricity variations, and not changes in obliquity, dominate variations in the solar insolation pattern at Titan—with up to a 1.4 AU difference between perihelion and aphelion, and complete cycling in the solar longitude of perihelion (L_{sp}, i.e. the time of season at which perihelion occurs). The calculation of orbital parameters in this work is identical to that described in Aharonson et al. (2009) and Appendix A of Lora et al. (2014), to which the reader is referred for a detailed treatment.

Because we quantify the influence of these orbital variations on the surface winds and dune orientations through computationally intensive GCM runs, a small but representative number of specific orbital configurations must be selected for study. We choose to focus on the four configurations for which the L_{sp} coincides with the solstices and equinoxes (referred to hereon as orbital extrema, Fig. 1a). For the two solstitial configurations, the locations of maximum solar insolation are maximally separated (i.e. in closest proximity to the south pole for $L_{sp} = 270°$, vs. the north pole for $L_{sp} = 90°$). As such, the changes in wind directions between these configurations are expected to be maximized (see Section 2.3.3). This cycling of L_{sp} occurs over a period of 45 kyr. We focus on the most recent cycle of the past 45 kyr, noting that the current orbital configuration in which southern summer occurs close to perihelion is most similar to the extremum of 2 kyr ago (we will refer to the orbital extremum of 2 kyr ago as the modern configuration). Note that the eccentricity of Saturn's orbit changes over this period as well, i.e. the perihelion distance also changes. Thus although the insolation patterns of the equinoctial extrema are equivalent, due to differences in the perihelion distance the total amount of solar radiation received varies for the autumnal and vernal equinox configurations.

We also consider a significantly longer cycle of order 1 Myr over the course of which each of the four extrema in L_{sp} of perihelion coincide with Saturn's maximum eccentricity of 0.09 (Fig. 1b).

2.2. General circulation model (GCM) descriptions

We run our simulations of the climatic conditions associated with these orbital extrema using three global, 3D GCMs: the Köln GCM (Tokano et al., 1999; Tokano, 2010), TitanWRF (Newman et al., 2011), and the Titan Atmospheric Model (TAM, Lora et al. (2015)). This is to identify those trends that are independent of the chosen model, and also investigate any model-dependent behavior. The models are described here briefly, although for greater detail the reader is referred to the indicated papers specific to each GCM. It is noted that all models use constant albedos and thermal inertias.

2.2.1. Köln GCM

The Köln GCM uses the Aries/GEOS dynamical core (Suarez and Takacs, 1994), and the radiative transfer scheme of McKay et al. (1989). The model extends up to 250 km altitude and includes 60 vertical layers, the lowest being at an altitude of 300 m. Its horizontal resolution is 11.25° longitude by 7.5° latitude. The surface roughness assumed by the model is 0.005 m, along with a thermal inertia value of 300 J m^{-2} $s^{-1/2}$ K^{-1}. The GCM is described in detail in Tokano 2008 and the references therein.

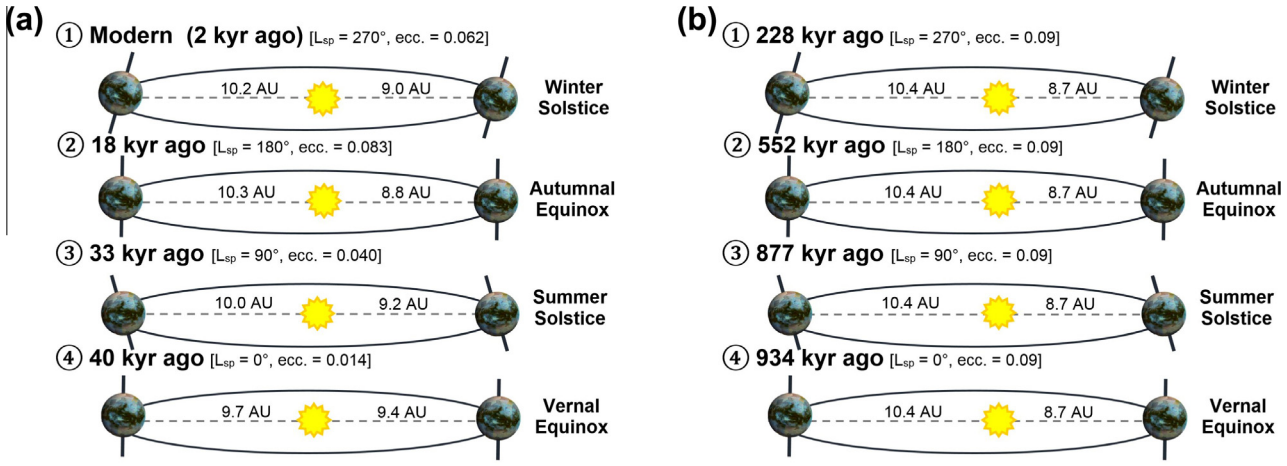

Fig. 1. (a) Extrema in Titan's solar longitude of perihelion (L_{sp}) over the past 45 kyr. The values for both the L_{sp} and Saturn's eccentricity (ecc.) are displayed for each configuration. (b) Extrema in Titan's L_{sp} coincident with the maximum eccentricity of Saturn's orbit. This cycle occurs over approximately 1 Myr (Image credit for Titan mosaic: Le Mouélic et al., 2010).

The Köln GCM has been used extensively in studies of Titan's tropospheric circulation (Tokano, 2009). In particular, this model has been used to investigate topographic effects on the wind regime (Tokano, 2008) and to imply a mechanism for generating eastward dune crest propagation through equinoctial fast westerly winds (Tokano, 2010).

2.2.2. TitanWRF

The TitanWRF v2 GCM is based on the PlanetWRF atmospheric model (Richardson et al., 2007) which is in turn based on the terrestrial Weather, Research and Forecasting (WRF) model v.3.0.1.1. The radiative transfer scheme is adapted from that of McKay et al. (1989). There are 54 vertical levels included in the model, up to 420 km altitude, with the lowest layer being at 85 m. The horizontal resolution is 5.625° longitude by 5° latitude. The model assumes a surface roughness of 0.001 m. The reader is referred to Richardson et al. (2007) and Newman et al. (2011) for detailed descriptions of the dynamical core. TitanWRF produces strong stratospheric superrotation, comparable to that observed (Newman et al., 2011), and has been used for predicting dune orientations and investigating the methane cycle.

2.2.3. Titan Atmospheric Model (TAM)

One of the newest Titan GCMs, the Titan Atmospheric Model (TAM) uses the Geophysical Fluid Dynamics Laboratory's Flexible Modeling System (Gordon and Stern, 1982). A novel radiative transfer scheme constrained heavily by recent observations is used by TAM—including methane absorption coefficients, a methane profile, and haze optical parameters as measured by the Huygens probe. The model includes 25 vertical layers, with the lowest layer being at 350 m, while the approximate horizontal resolution for this spectral model is 5.625° longitude by 5° latitude. A surface roughness of 0.005 m is assumed by the model, along with a thermal inertia value of 335 J m^{-2} $s^{-1/2}$ K^{-1}. Lora et al. (2014) describe the model parameters in greater detail, although we note that the specific orbital configurations used in that paper differ slightly from those presented here.

TAM has previously been used to study the climate forcing of the Croll–Milankovitch cycles, although with focus on methane transport (Lora et al., 2014). A more recent configuration of the model with higher vertical resolution has improved stratospheric superrotation (Lora et al., 2015). Although the model runs for the orbital extrema presented here utilize the Lora et al. (2014) configuration of TAM (TAM L25), additional runs using the most recent 32 layer model (TAM L32) were carried out for statistical analyses (Supplementary Information, Section 1).

2.3. GCM runs

Two different types of runs are carried out on the models described in the previous section: runs of the models that do not include surface topography, and those that include large-scale topography. Only TitanWRF is run in both configurations.

The methane hydrologic cycle is not included in the runs. Charnay et al. (2015) suggest that the detailed, small-scale circulation in the vicinity of methane storms may explain the observed low latitude eastward sand transport, but this effect cannot be captured in the lower resolution of global models. Furthermore, the inclusion of methane hydrology would introduce additional uncertainties to the modeling, arising in particular from the currently unknown surface distribution of methane (Neish and Lorenz, 2014). Assumptions on the surface methane distribution affect the latitudinal extent of the Hadley circulation and the timing of its seasonal reversal (Mitchell et al., 2006, 2009; Lora and Mitchell, 2015), neither of which are unambiguously constrained by observation (Lebonnois et al., 2014). Models that assume an extensive global surface methane reservoir produce surface temperatures that are too low with respect to Cassini Composite Infrared Spectrometer (CIRS) surface brightness temperature observations, when compared with models that only include deep polar reservoirs (effectively dry simulations at low and mid latitudes) or dry simulations (Jennings et al., 2011; Lora et al., 2015). To reduce uncertainties in the general circulation associated with assumptions about the surface methane distribution, and facilitate inter-model comparisons, we focus on the effects that orbital changes have on the large-scale dry circulation. We also note that all previous GCM studies of the dunes have used dry simulations. The simulations presented herein account for dry convection: the Köln GCM utilizes the dry-convective adjustment scheme of Manabe et al. (1965), TitanWRF makes use of the Medium Range Forecast (MRF) vertical diffusion parameterization scheme (Hong and Pan, 1996), and TAM includes vertical diffusion of heat and momentum within the planetary boundary layer through a nonlocal K-profile scheme (Lora et al., 2015).

The spin up of the models all begin with a dry, resting atmosphere. The time for the spin up simulations are: 1–2 Titan years for the lower troposphere of the Köln GCM, 65–70 Titan years for TitanWRF to achieve a state of realistic stratospheric superrotation,

and 10 years for TAM L25 which is then run for additional years for high-frequency output. At the end of spin up, the Köln GCM has a thermal profile that is overall slightly warmer than observation albeit in good agreement in the lower troposphere, TAM shows close agreement with the Huygens profile in the troposphere, and TitanWRF has a thermal profile with a 5–10 km offset lower in altitude compared with that measured by Huygens.

Runs are carried out for each of the orbital extrema, and are run for one Titan year after spin-up. With no methane cycle and the resolution of a global model, significant interannual variability is not expected at low latitudes. The winds from the model are sampled at a high temporal cadence (24 or 48 times per Titan day, one Titan day is 15.95 Earth days) so as to accurately capture diurnal effects. For consistency, in all models, the winds from the lowest vertical grid point are scaled down to a height of 10 m using the law of the wall (von Kármán, 1930) to represent surface winds:

$$U(z) = \frac{u_*}{\kappa} ln \frac{z}{z_o} \quad (1)$$

where u_* is the friction velocity, $\kappa = 0.41$ is the Von-Kármán constant (Garratt, 1977), z is the height above the surface, and z_o is the roughness length assumed by the particular GCM. Use of the law of the wall in this scaling is justified by the lowest layer of each GCM being at or below the 300 m to several km high planetary boundary layer that has been suggested for Titan (Tokano et al., 2006; Lorenz et al., 2010; Charnay and Lebonnois, 2012) The surface winds from these runs are then used to determine a predicted dune orientation (see Section 2.4).

2.3.1. Runs without topography

Both TitanWRF and TAM are run in configurations without topography. The scaled surface wind outputs are analyzed across the equatorial region (all longitudes within 20° latitude of the equator). Wind outputs are recorded 24 times per Titan day over the course of the one Titan year (29.4 Earth years) runs. Both GCMs are run for all four orbital extrema in the 45 kyr L_s of perihelion cycle, while only TitanWRF is also run for the configurations of the 1 Myr L_s of perihelion at maximum eccentricity cycle.

Because these GCMs do not include topography, their predicted dune orientations are not expected to closely match observation. However, the lack of topography does not preclude calculating predicted dune orientations, for which variations as a function of the orbital configuration can still be attributed to changes in the general circulation. It is noted that the lack of topography and the assumption of spatially uniform surface albedos and thermal inertias do not force longitudinal asymmetries in these runs. Saturn's gravitational tides, which are included in TitanWRF, may cause some longitudinal asymmetries in that model because of the dependence of tidal potential on longitude. However these tidal asymmetries are minor, especially at low latitudes (Tokano, 2008). These runs are thus largely longitudinally symmetric, allowing for certain statistical analyses on the computed dune orientations. Namely, within a latitudinal band, dune orientations are calculated at 64 different longitudinal grid points, each with the same initial conditions. For this reason, the differences in dune orientations within a zonal band can be used to examine inherent variability within a given run. Accordingly, zonal statistics (means and standard deviations) are calculated for the dune orientations of each model run. The means are reported as the predicted dune orientations for a given latitude. Within a zonal band for a particular epoch, the standard deviations in dune orientations can be compared with the variability of the orientations for runs of the different orbital extrema. This allows for evaluation of whether changes in the orbital parameters result in differences in the dune orientations that are statistically significant compared to the inherent variability of the model.

2.3.2. Runs with topography

TitanWRF and the Köln GCM are run with the effects of surface topograhy included. Both models utilize the ellipsoid of Iess et al. (2010) which is subtracted from the topography map of Lorenz et al. (2013) for TitanWRF and the global shape model of Zebker et al. (2009) for the Köln GCM. The latter shape model is used in the Köln GCM for consistency with the results outlined in Tokano (2010), such that the model runs presented here differ from that work only in the orbital parameters. Surface wind outputs are recorded 24 times per day for TitanWRF and 48 times per Titan day for the Köln GCM. Annual runs for all four orbital extrema in the 45 kyr are carried out by both GCMs, while only the Köln GCM is also run for the 1 Myr cycle. Note that the TitanWRF simulations with topography presented here have weakened stratospheric superrotation compared to the simulations without topography. This appears to be due to stratospheric breaking of gravity waves triggered by the surface topography, and may result in weaker near-surface wind speeds than would otherwise occur in this run. Work is underway to examine and remove this largely spurious effect.

Predicted dune orientations are calculated based on the scaled surface winds from these runs, at single grid points corresponding to well developed regions in Titan's five major sand seas (Fensal, Shangri La, Belet, Senkyo and Aztlan). No zonal statistics are calculated for these runs, as the topography is a forced longitudinal asymmetry, and results will be a function of longitude as well as latitude. The dune orientations calculated from these GCM runs are then compared with observations.

2.3.3. Comparison of the GCM wind regimes

Seasonal wind rose diagrams for each of the GCMs run in the modern orbital configuration, are shown for the location of the Fensal sand sea in Fig. 2. With regards to meridional winds, the general trend of southerlies from L_s 0–180° and northerlies from L_s 180–360° is seen across all GCMs and is associated with the seasonal reversal of Titan's single, cross-equatorial Hadley cell. Although the equinoctial and solstitial seasons have similar cross-equatorial wind regimes, the winds during the latter are typically stronger due to the associated asymmetrical solar forcing. The greater windspeed of the northerlies over the southerlies across all GCMs can be associated with the modern day seasonal asymmetry of Titan's orbit—in which winter occurs near perihelion, strengthening the solar forcing of this season's wind regime (Lora et al., 2015). Note that unless specifically stated otherwise, all seasonal references are to those occurring in the northern hemisphere.

In the equatorial region, the greatest differences among the GCMs is in the zonal winds. Only the Köln GCM produces westerlies as its majority of highspeed winds (Fig. 2d, winds greater than 0.8 m/s for L_s 180–270°), which are associated with reversal of the meridional pressure gradient at equinox (Tokano, 2010). In addition, the spring/summer southerlies of both of the models including topography have a significant westerly component to them—this effect is attributed to topographic influence. For the runs without topography, while the southerlies in TAM have a fraction with a westerly component to them, westerlies are almost altogether absent in TitanWRF.

Because surface wind velocity measurements have only been recorded in one location on Titan, by the Huygens probe (Bird et al., 2005; Karkoschka, 2016), they are poorly constrained and the windspeeds are another source of variability among the GCMs (visible in the proportions of the various colors in the wind roses of Fig. 2). The highest peak wind speeds are found in the Köln GCM, although they are extremely rare and as such are not visible in the wind roses shown. The windspeed distribution in TitanWRF is broader and shifted towards higher winds overall. TAM rarely has surface winds exceeding 0.8 m/s.

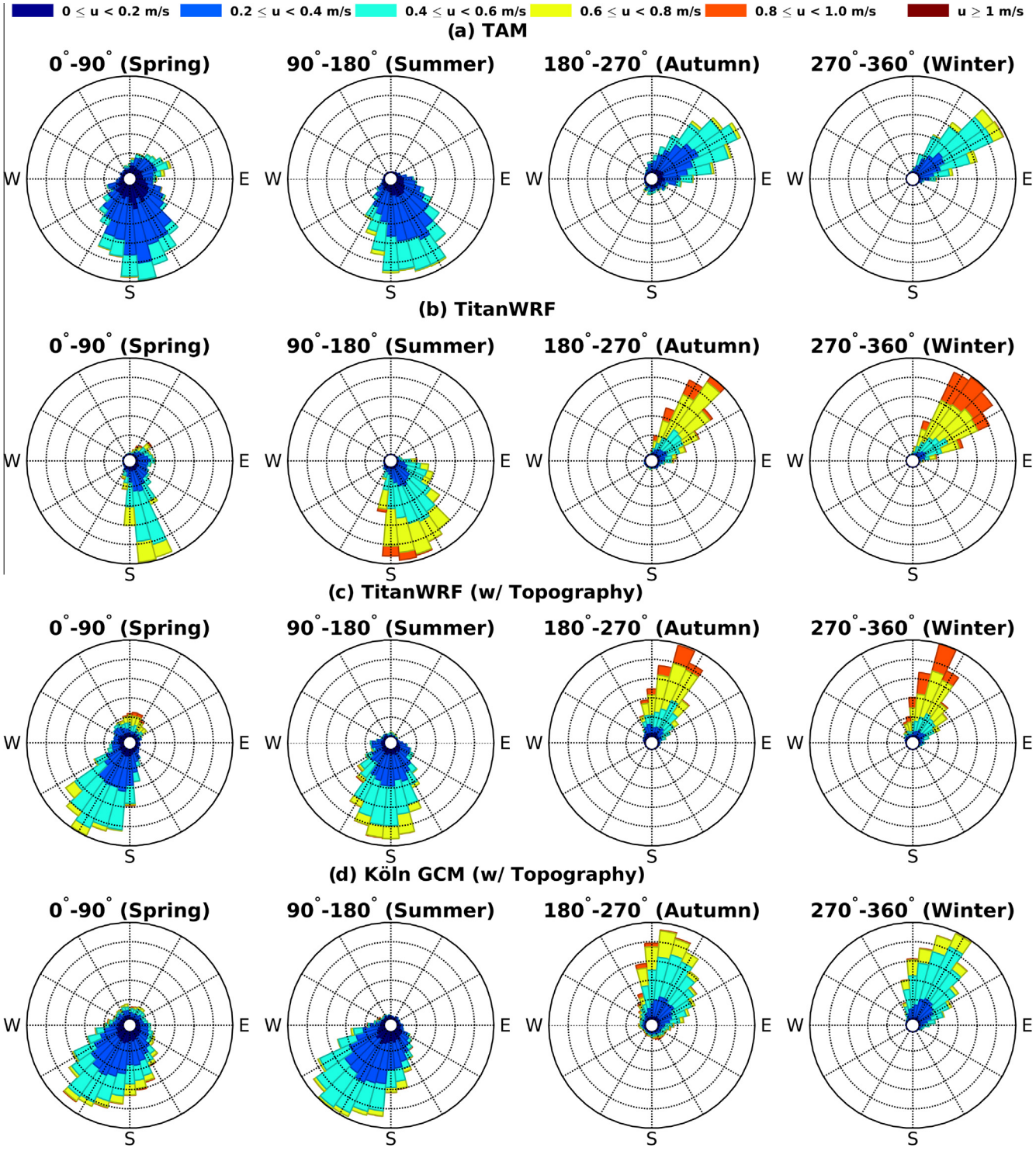

Fig. 2. Seasonal changes in the wind regime for annual runs of the modern epoch at the Fensal sand sea for all GCMs. The L_s binning for the seasons is indicated above the wind roses. Each bin represents the number of winds blowing from that direction, with the radius proportional to the frequency and the color indicative of the wind speed. The grid points for the GCMs are as follows: TAM 8.3°N 56.25°W, TitanWRF 7.5°N 53.44°W, Köln GCM 7.5°N 56.25°W. The fact that the spring and summer southerlies have a greater westerly component for both models incorporating topography suggest that these westerlies are topographically driven. (For interpretation of the references to color in this figure legend, the reader is referred to the web version of this article.)

2.4. Sediment transport relation and model for dune orientations

Given the annual regime of near-surface winds at any given grid point in the GCM, the predicted dune orientation and direction of dune propagation can be calculated by using dune formation theory. We define an orientation to be the azimuthal (clockwise from north) positioning of the dune crest between 0° and 180°. This orientation is not a vector in the sense that there is no information concerning the elongation direction for linear dune crests (e.g. an orientation of 90° and 270° would be considered equivalent). We define the propagation direction of the dune crest to be the full vector between 0° and 360° azimuth, breaking the symmetry that

is present for just the orientation. The necessity for this distinction arises from the methods outlined below which require initial calculation of a dune orientation before the propagation direction.

To calculate dune orientations, we focus on the method of maximum gross bedform-normal transport. Dunes of a wide range of morphologies have been shown in both laboratory and field experiments to assume a crestline orientation such that the amount of sediment transported perpendicular to the crests, in both directions, is maximized (Rubin and Hunter, 1987; Rubin and Ikeda, 1990; Ping et al., 2014). We refer to this orientation as the gross bedform-normal transport (GBNT) orientation, which is associated with systems that are transport-limited, i.e. sediment is mobile and its movement is limited by the transport capability of the winds (Courrech du Pont et al., 2014). Morphologic and spectral evidence supports that large regions of Titan's sand seas are transport-limited (Lorenz et al., 2006; Radebaugh et al., 2008, 2010; Le Gall et al., 2011; Rodriguez et al., 2014). However, we note that the data cannot exclude the sediment availability-limited case (i.e. that sediment is mobile, but not at transport capacity) in all regions, for which consideration of an alternative mechanism for determining the dune orientations would be necessary (Courrech du Pont et al., 2014; Lucas et al., 2015).

To construct a dune orientation based on a multimodal flow, we begin by calculating the gross bedform-normal transport for all dune orientations between 0° and 180° with a step size of 0.5°. The orientation for which the gross bedform-normal transport is maximized is the GBNT orientation. Calculation of gross-bedform normal transport requires use of a sediment transport model. For its previous application to non-terrestrial environments, we use the mass flux relation derived in White (1979):

$$T = K \cdot \frac{\rho_a}{g} \cdot u_*^3 \cdot \left(1 - \frac{u_{*c}}{u_*}\right) \cdot \left(1 + \frac{u_{*c}}{u_*}\right)^2 \quad (2)$$

where T is the mass flux in kg m s^{-1}, K is an empirical non-dimensional constant typically set to 2.61, ρ_a is the air density, g is the gravitational force, u_* is the magnitude of a surface wind velocity converted to a shear velocity, and u_{*c} is the threshold shear velocity for saltation. Note that this relation can only be used for winds greater in magnitude than the saltation threshold ($u_* > u_{*c}$), otherwise no transport is expected. It is unknown whether the empirical constant K should have a similar value under the different physical environment of Titan as is assumed on Earth and Mars. Furthermore, the effect of the low density of Titan's inferred hydrocarbon sediment (Clark et al., 2010) on this transport relation is neither explicitly accounted for nor obvious. For this reason, we utilize a modified version of the White 1979 relation, in which we remove K, and g. Because we are using relative differences in these fluxes to determine a predicted dune orientation, with the assumption that these parameters do not vary temporally, the reported orientations are not affected by this simplification. We also exclude ρ_a in our calculations, as inclusion of this parameter was found to consistently affect our predicted dune orientations by less than half of a percent. Thus we are computing a proxy for mass flux. We calculate the gross-bedform normal transport for each possible dune orientation α between 0° and 180°:

$$T_p(\alpha) = \sum_i \left| sin|\alpha - \beta_i| \cdot u_{*i}^3 \cdot \left(1 - \frac{u_{*c}}{u_{*i}}\right) \cdot \left(1 + \frac{u_{*c}}{u_{*i}}\right)^2 \right| \quad (3)$$

where T_p is the proxy for mass flux, u_{*i} is the friction velocity at the surface, and β_i is the direction of the wind whose magnitude is u_{*i}. Note that we are summing over the index i, to account for all model wind outputs over one Titan year where $u_{*i} > u_{*c}$. The absolute value in the sine expression accounts for situations in which β_i is less than α, while the absolute values around the whole expression are necessary as the method of GBNT considers all fluxes perpendicular to the dune crest as contributing. The angle α for which T_p is maximized is the predicted dune orientation.

Although an orientation has now been calculated, there is no information about a propagation direction. We calculate this direction using the concept of the resultant drift direction (RDD, Fryberger and Dean (1979)), in which drift potentials, or transport fluxes, are calculated in each direction from 0° to 360°, (again with a step size of 0.5°, making our implementation differ from that of Fryberger and Dean (1979) where drift potentials were only calculated in 16 directions). The vector sum of these drift potentials then provides the RDD. The RDD is thus a net sediment transport direction. In calculating the drift potentials, we use the same proxy for mass flux T_p in Eq. (3), noting that for the RDD α is not a tested dune orientation but the direction for which we would like to measure mass flux, and thus we replace the sine function in Eq. (3) with a cosine. α is varied the full 0° to 360°, in turn only wind contributions blowing in the same direction as the drift direction of interest are summed (i.e. the absolute value signs in Eq. (3) are removed, and any terms with a negative contribution are removed from the calculation). The vector sum of the T_p values for all angles α is the RDD. The GBNT dune orientation provides two possible directions of propagation (e.g. 90° or 270°). The propagation direction in closer alignment with the RDD is chosen, and determines whether the dune is propagating eastward or westward.

Note that the saltation threshold u_{*c} appears in the mass flux calculations. The saltation threshold for the grains composing Titan's dunes is not known. Recent experimental work has suggested thresholds that are high with respect to the winds measured and modeled on Titan (Burr et al., 2015). However, the unknown nature of the exact chemical composition of the dune grains, and in turn both their physical properties and tendency for cohesion precludes determination of a precise empirical value for this threshold. An added complication is the distinction between the thresholds measured in wind tunnels and those determined from mesoscale and global climate models. The low resolutions in these models preclude capturing the finest scale wind features such as eddies and associated gusts, such that the winds output from these models best represent averages of the winds over the GCM grid cell. These effective averages over areas hundreds of square kilometers in area will naturally result in the calculation of thresholds that are lower than measurements from wind tunnels, which include the effects of the finest scale winds (Ayoub et al., 2014). For these reasons, estimates of the saltation threshold (quoted as free-stream wind speeds at 10 m, assuming a surface roughness z_o = 0.005 m) on Titan vary, including 0.7 m/s from matching observations in a GCM (Tokano, 2010; Lucas et al., 2014; Charnay et al., 2015), 0.5–1.1 m/s using model expressions for the saltation threshold, with a variety of interparticle force parameters (Lorenz, 2014), and 1 m/s from modifying a saltation threshold model to match experimental results (Burr et al., 2015). As a result of both the large range of estimated thresholds, and the complications which arise in comparing thresholds derived from GCMs and experimental work, dune orientations in this work are presented as a function of the currently unconstrained saltation threshold.

The sediment mass flux in Eq. (2) is roughly dependent on the cube of the windspeed. Thus the highest speed winds can control dune orientations—and their weighting increases further when the saltation threshold is raised and increasingly higher speed winds are disregarded in the calculation.

2.5. Mapping of dune orientations in Cassini RADAR data

The dune orientations predicted by the GCMs which include topography can be compared with observations. For this

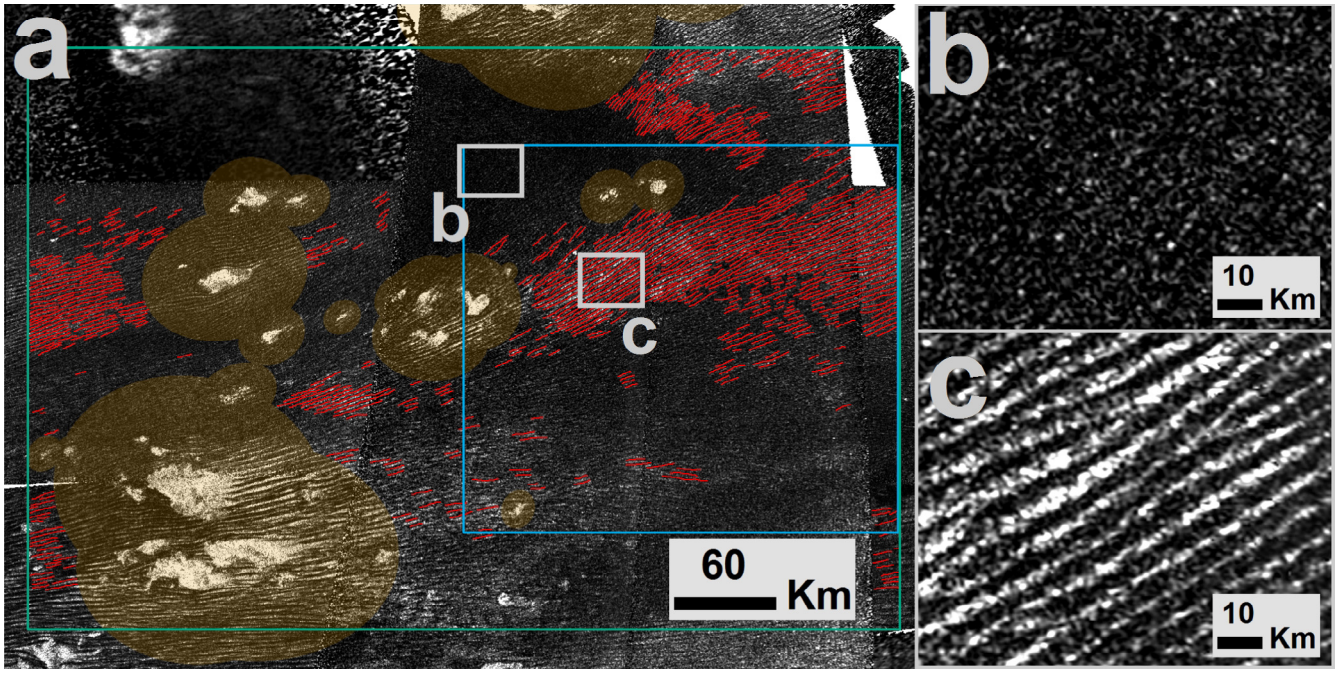

Fig. 3. (a) Dune orientations (red) mapped within the Köln GCM grid (green, centered on 7.5°S, 247.5°W) and the TitanWRF GCM grid (blue, centered on 7.5°S, 244.69°W) corresponding to the Belet sand sea. Topographic obstacles below the resolution of the models are treated as ellipses, and dunes within one semi-major axis distance of these obstacles (yellow) are not mapped to avoid incorporation of highly localized orographic effects when comparing with GCM predictions. Regions that are not mapped correspond either to areas of low data quality, or to degraded dunes as shown in panel (b). These are contrasted with long unbroken crestlines greater than 10 km in length, as shown in panel (c). (For interpretation of the references to color in this figure, the reader is referred to the web version of this article.)

comparison, we map dunes within the GCM grids corresponding to well developed regions of the five major sand seas. Dunes are mapped in the high-resolution (as high as 250 m per pixel, Elachi et al. (2005)) synthetic aperture radar (SAR) images constructed from observations of the Ku-band Cassini RADAR instrument.

An example of dunes mapped within the GCM grids of TitanWRF and the Köln GCM in the Belet sand sea are shown in Fig. 3. Long, unbroken dune crestlines over 10 km in length are mapped (Fig. 3c). Regions corresponding to degraded dunes are not mapped (Fig. 3b) due to both ambiguity in the orientations and their possible association with moisture-cohered sediment (Ewing et al., 2015). We also do not map dunes in the vicinity of sub-grid scale topographic obstacles to prevent including dunes influenced by highly localized orographic effects. These are effects that would not be captured by the coarser topography included in the GCMs. We treat the dune obstacles as ellipses and measure their semi-major axes. Those dunes that are within a distance equal to this semi-major axis from the obstacle are considered to be influenced by the obstacle's effects on the winds. This criterion was effective across the sand seas in excluding those dunes observed to be streamlining around the obstacles. It is noted that due to low resolution data in the Aztlan sand sea, in order to accumulate a statistically significant sample of dune crests, we map dunes in the neighboring GCM grids in addition to those in the grid point of interest.

3. Results

We present the surface winds and resultant dune orientations predicted by annual runs of the three GCMs. First we present results for the 45 kyr solar longitude of perihelion (L_{sp}) cycle, followed by those for the 1 Myr L_{sp} at maximum eccentricity cycle. The results for each cycle are subdivided into those for the GCM runs without and with topography.

3.1. 45 kyr L_s of perihelion cycle

3.1.1. Wind regimes

The annual GCM wind distributions at the Fensal sand sea for the 4 orbital extrema are shown in Fig. 4. Note the balance of northerly and southerly winds; this results in the prediction of approximately east–west dune orientations (as GBNT involves maximizing the transport perpendicular to the dune crests). Although there are no radical changes in the general circulation caused by the orbital precessions, the subtle alterations to the wind regime that do result, especially with regards to the high-speed winds, can have significant effects on the dune orientations.

A trend visible in both runs of TitanWRF and the Köln GCM is shifts in the proportion of the strongest winds that are northerly or southerly between the modern orbital configuration and that of 33 kyr ago—the high-speed southerlies being more prevalent for the latter orbital epoch. This difference between the epochs can be associated with the nature of the seasonal asymmetries. At present winter solstice coincides largely with perihelion, while 33 kyr ago summer solstice coincided exactly with perihelion (Fig. 1a). The strongest winds are thus associated with the wind regime of the perihelion season. Note that due to differences in the zonal orientation of the southerlies and northerlies, this also results in a shift in direction of the strongest zonal winds, which are largely westerly in the case of 33 kyr ago in the Köln GCM, and partly westerly for the corresponding run of TitanWRF with topography. Thus for 33 kyr ago, in the Köln GCM the GBNT dune propagation direction at the Fensal dune field is consistently eastward, and eastward for higher saltation thresholds of the topography run of TitanWRF (see Section 3.1.3 and Fig. 6). The wind regimes for the extrema $L_{sp} = 0^\circ$ (18 kyr ago) and $L_{sp} = 180^\circ$ (40 kyr ago) are not equivalent due to differences in the perihelion distance, as described in Section 2.1.

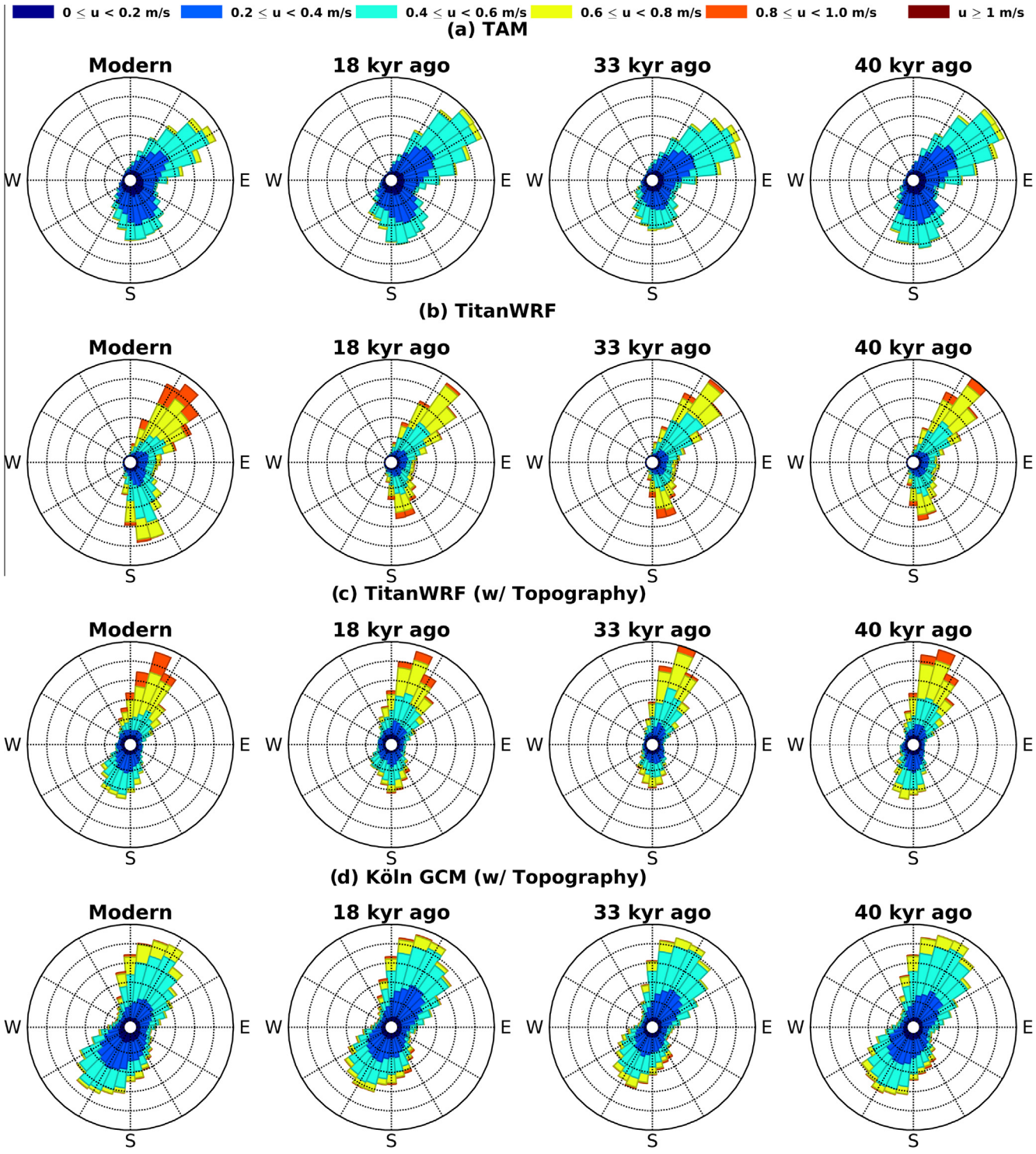

Fig. 4. Changes in the annual wind regime at the Fensal sand sea as a function of the orbital configuration (in the 45 kyr L_s of perihelion cycle), for all GCMs. The plotting conventions are the same as Fig. 2. The GCM grid point coordinates are the same as those in Fig. 2. Although no radical effects on the general circulation arise from changes in the orbital configuration, changes in the ratio of northerlies to southerlies, and variability in the high speed winds are observed among the orbital extrema.

3.1.2. Dune orientations for runs without topography

Fig. 5 displays the GBNT dune orientations for TitanWRF and TAM. Each axis represents a different zonal band within 20° of the equator. The colored lines within an axis indicate the zonal averages of the dune orientations for the orbital extrema, while the shaded error bars denote 1σ deviations. Orientations are also calculated for a combined wind regime approximating that of the full orbital cycle. This is determined by combining the winds from the annual runs for each of the orbital extrema into one four-year wind distribution, and predicting a dune orientation. These approximate the orientations that would be expected should the reorientation timescale of the dunes be greater than 45 kyr—whereby the wind regime of the entire 45 kyr cycle would contribute to the dune orientations. When a line terminates before the highest saltation threshold on the axis, it is due to the lack of winds in its corresponding orbital run that are higher in velocity

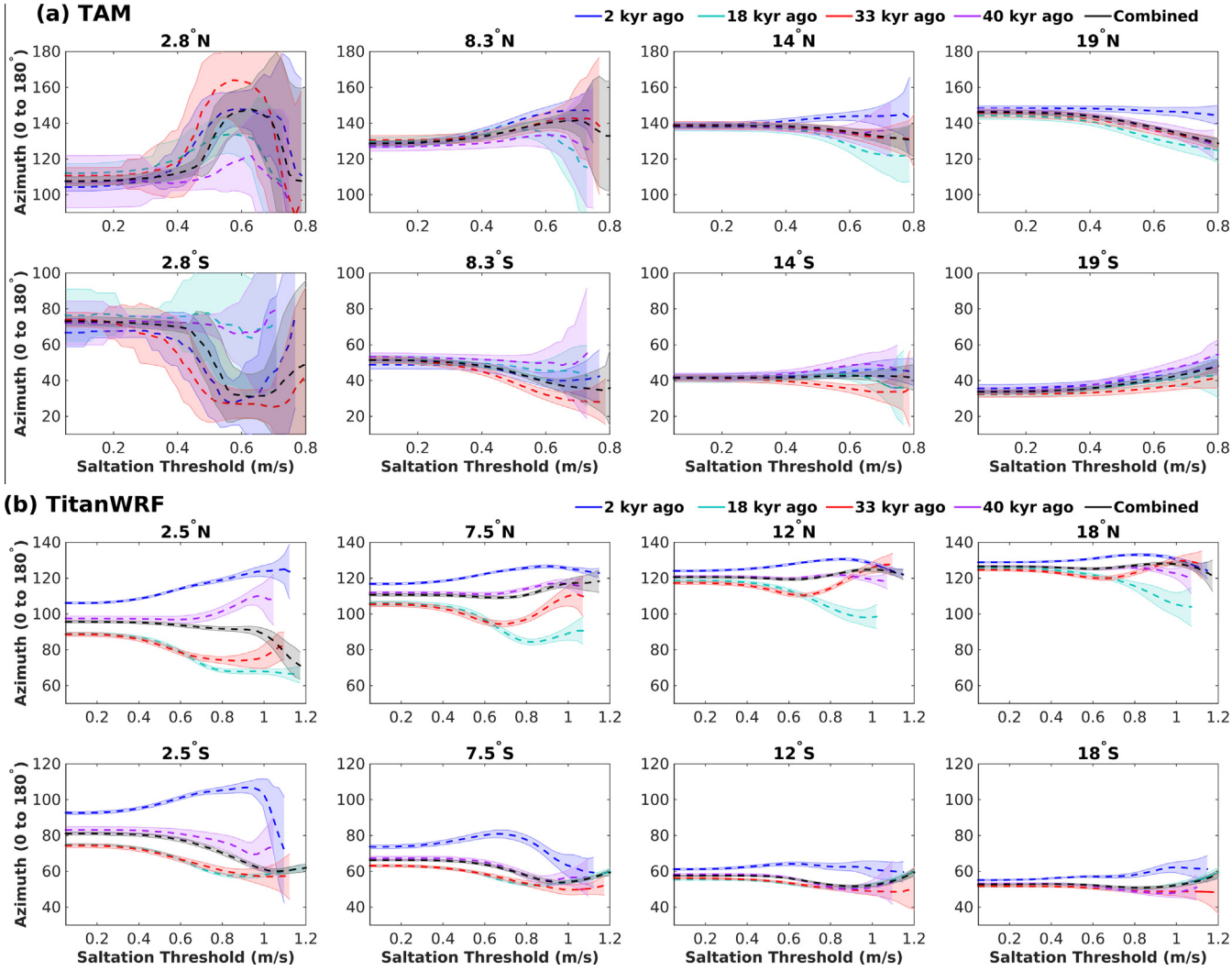

Fig. 5. Zonally averaged GBNT dune orientations as a function of the free-stream saltation threshold for the (a) TAM and (b) TitanWRF runs without topography. Each plot represents a different latitude. The colored lines within each plot represent mean dune orientations for the different orbital epochs of the 45 kyr L_s of perihelion cycle, with the shaded regions denoting 1σ deviations. Dashed lines indicate westward propagation of the dunes while solid lines represent eastward propagation. Although the minimum and maximum values of the *y*-axis may vary, the ranges are identical for all of the *y*-axes. Note the difference in the *x*-axis ranges among the two GCMs, which is necessary due to the variations in the maximum windspeeds of the models. (For interpretation of the references to color in this figure legend, the reader is referred to the web version of this article.)

than this termination point. Note that these orientations are presented as a function of the free-stream saltation threshold (i.e. the corresponding wind velocity 10 m off the ground necessary to saltate grains), although the orientations were calculated using shear velocities. Due to the periodic nature of the data, the parameters calculated for the dune orientations are circular means and circular standard deviations. We calculate these parameters for the orientations as opposed to the propagation directions, as those for the latter can present unintuitive results (e.g. the circular mean of the propagation directions 90° and 270° is 180°, despite this direction being orthogonal to both the inputs. Calculation using the orientations presents means that are in close alignment with the input orientations). The propagation directions of the means are in turn presented as dashed lines representing westward propagation, and solid lines representing the eastward propagation that is found in all observations of Titan.

In the case of TAM, some variability in the GBNT orientations among the epochs is seen (Fig. 5a). For most latitudes, the orientations of the different epochs are within one standard deviation of one another. Nevertheless, for intermediate saltation thresholds, the orientations for 33 kyr ago differ from the other orbital extrema at 8.3°S and 14°S, as do the modern dune orientations at 14°N. Furthermore, the modern orientations at 19°N differ from those of the other epochs for all saltation thresholds above 0.1 m/s. An epoch can thus uniquely define a dune orientation in certain cases. It is noted that there is considerably greater longitudinal variation in the dune orientations at 2.8°S and 2.8°N in comparison with the higher latitudes (visible in the magnitude of the standard deviations). This variability is associated with greater longitudinal variability in the wind regime within these zonal bands—specifically changes in the ratios of northerlies to southerlies. This may be due to movement or longitudinal variation in the location of the intertropical convergence zone at equinox, which would affect at each location the proportion of winds associated with the circulation of the northern vs southern hemisphere. Another trend that is observed is an increase in the differences among the dune orientations as the saltation threshold is raised. This is the result of two effects. At higher saltation thresholds proportionately

fewer of the low speed winds, which are largely consistent between orbital extrema (blue[1]-shaded areas in the rose diagrams of Fig. 4), are used in determining the orientations. Concurrently, the higher speed winds have greater directional variability between the extrema. The result is that at high saltation thresholds, the sampled portions of the wind regimes of the different epochs are more disparate. Most of the dunes are propagating westward, except for isolated cases such as for high saltation thresholds 18 kyr ago at 14°S where eastward propagation (the direction consistent with observation) is found.

In the case of TitanWRF (Fig. 5b), consistent differences in the GBNT dune orientations predicted for the orbital extrema are seen across latitudes. These differences can approach 50° (see the axes for 2.5°N and 2.5°S latitude). In TitanWRF, consistent differences between the zonally averaged dune orientations of the different epochs are also seen at the 2σ level. The same trend as that seen in TAM of increasing differences in the dune orientations as a function of the saltation threshold is found at most latitudes. Note however that except for two isolated examples, 33 kyr ago at thresholds of 1.1 m/s at 7.5°S and 18°S, the dunes are propagating westwards, in conflict with observation.

The tendency for the differences in the dune orientations among the epochs to increase as a function of the saltation threshold requires verification that this effect is not due to small sample sizes in the wind distributions. This is because as the saltation threshold is raised, a narrower range of wind speeds is being sampled from the wind distribution. Therefore, there exists the possibility that the differences in the orientations of the epochs are simply due to sampling errors from wind distributions that are in fact close to identical. To investigate this, we analyze dune orientations calculated from subsamples of the GCM runs, and from multiyear simulations at the same orbital configuration. We find that the variability in dune orientations between subsamples (or separate years of a multiyear run) for the same orbital configuration is small, and considerably less than the differences between the orientations of the epochs. That is, the differences in dune orientations between epochs is indeed due to differences in the wind regime and not an issue with insufficient sample sizes (Supplementary Information, Section 1).

3.1.3. Dune orientations for runs with topography

The GBNT orientation results for the GCM runs which include topography are shown in Fig. 6. The plotting conventions are similar to those in Fig. 5 with the exception that each axis represents a single GCM grid point corresponding to a location within one of the five major sand seas (as opposed to a zonal band), and thus the lines represent dune orientations at a single location (not zonal averages). The histograms denote the orientations of all well-organized dune crests mapped in RADAR data within the GCM grids, with the total number (n) of mapped dunes displayed above each axis.

For TitanWRF, variability in the dune orientations of 5–10° is found for most cases between epochs, although differences of 20° and 50° are found at the Aztlan and Shangri La sand seas respectively. While westward dune orientations dominate, as was the case for the run without topography, predominantly eastward dune orientations are found both in Belet and Aztlan and for high saltation thresholds for 2, 33 and 40 kyr ago at Fensal (as anticipated based on the wind regime described in Section 3.1.1). The large variations in dune orientations at Shangri La are a result of this site being the most sensitive to the changes in the ratios of northerlies to southerlies associated with the seasonal asymmetries of the epochs (as discussed in Section 3.1.1), although the lack of westerlies at this site results in almost purely westward transport (the exception being 33 kyr ago at a 0.9 m/s threshold).

The variability among the epochs is comparable for the Köln GCM, where differences of up to 70° (as seen in the Fensal sand sea) are seen among the dune orientations. However, significant variability in the magnitude of this effect is apparent among the sand seas. The large differences in the dune orientations at Fensal in this model is partially attributed to greater variability in the directions of the highest speed winds among the epochs when compared with other sites. Consistent with the results for the GCMs without topography, the differences between the orientations of the epochs generally increases as the saltation threshold increases. A mix of eastward and westward propagation directions are seen, however the eastward propagation direction in agreement with observation can be achieved for certain epochs and thresholds in all sand seas with the exception of Senkyo.

There is close agreement between the modeled and observed GBNT dune orientations for three out of the five sand seas for both TitanWRF and the Köln GCM (Fensal, Belet and Senkyo for the former, and Fensal, Shangri La and Belet for the latter). With the exception of Senkyo in the Köln GCM, the correct eastward propagation direction can be achieved at high saltation thresholds for specific epochs. This in combination with certain cases where the orientations differ sufficiently among the epochs, can point to specific epochs being in greatest agreement with observation (e.g. for TitanWRF: 33 kyr ago at Fensal and Senkyo, for the Köln GCM: 33 kyr ago at high thresholds in Shangri La, 33 kyr ago at intermediate saltation thresholds or 40 kyr ago at high saltation thresholds for Fensal, 18 kyr ago at Belet). There is also reasonable agreement between observation and the orientations for the wind regime combining all four epochs, where the correct orientations and eastward propagation can be achieved at Belet and Fensal for both GCMs. The GBNT dune orientations or propagation directions in Shangri La and Aztlan are mostly in disagreement with observation in both GCMs.

3.2. 1 Myr L_s of perihelion cycle at maximum eccentricity

3.2.1. Dune orientations for runs without topography

TitanWRF was the only model run with the configurations of the 1 Myr cycle without topography. The predicted orientations are displayed in Fig. 7. The general trend of the differences between the orientations of the epochs are similar to those described for the 45 kyr cycle in Section 3.1.2 and seen in Fig. 5a. However, in most cases the differences between the dune orientations for the 1 Myr cycle are greater than the differences for the 45 kyr cycle. This is particularly apparent in the splitting of the orientations for the three extrema corresponding to autumnal equinox, summer solstice and vernal equinox at 7.5°S, 12°S and 18°S, for which the analogous extrema in the 45 kyr cycle were clustered.

3.2.2. Dune orientations for topography runs

The orientations for the 1 Myr cycle runs of the Köln GCM are shown in Fig. 8. Although there are many similarities with the orientations predicted by this model for the 45 kyr cycle (described in Section 3.1.3 and seen in Fig. 6), there are important differences. Firstly, note the change in the range of saltation thresholds for which the orientations in Fig. 8 are displayed. Orientations can be calculated for higher saltation thresholds in the 1 Myr cycle in comparison with the 45 kyr cycle, due to faster winds being generated by the model for the orbital configurations of the former (this is a result of the increased solar input due to the smaller perihelion distances of 8.7 AU for all extrema of the 1 Myr cycle, Fig. 1b). Other differences from the 45 kyr cycle include closer agreement among the orientations for the different epochs at both Fensal

[1] For interpretation of color in Fig. 4, the reader is referred to the web version of this article.

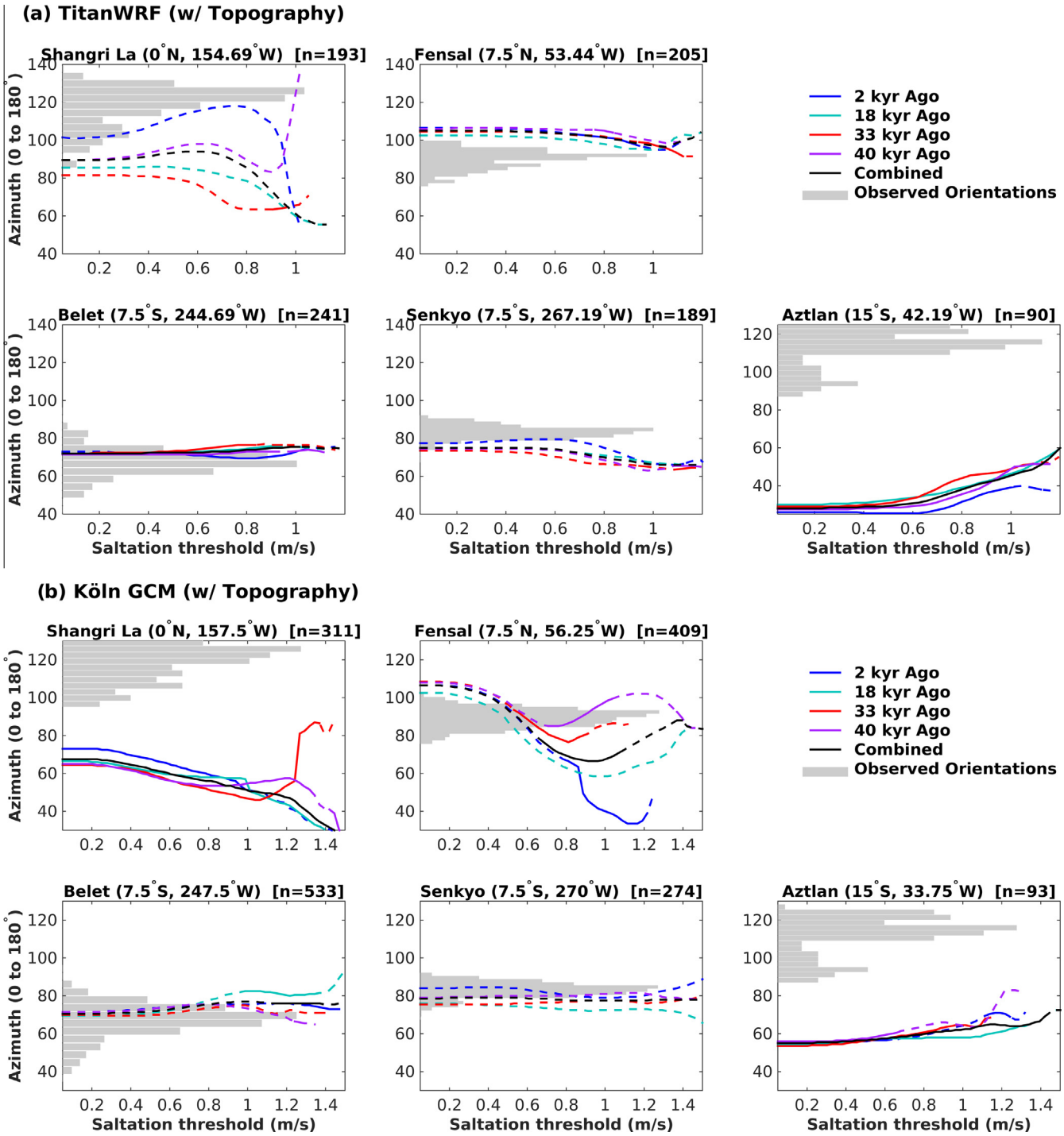

Fig. 6. GBNT dune orientations as a function of the free-stream saltation threshold predicted by the model runs incorporating topography: (a) TitanWRF and (b) the Köln GCM. Each of the five axes correspond to well-developed regions of one of the five major sand seas. The different colored lines within each plot denote predicted dune orientations for the orbital epochs of the 45 kyr L_s of perihelion cycle. Dashed lines denote westward propagation of the dunes while solid lines indicate eastward propagation. The histograms denote observed dune orientations mapped in Cassini RADAR data, within the corresponding GCM grids. The total number of mapped dunes are displayed in the number n above each plot. Although the minimum and maximum values of the y-axis may vary, the ranges are identical for all of the y-axes. Note the difference in the x-axis ranges among the two GCMs, which is necessary due to the variations in the maximum windspeeds of the models. (For interpretation of the references to color in this figure legend, the reader is referred to the web version of this article.)

and Shangri La. Agreement with observation improves over the 45 kyr cycle in that at high saltation thresholds the correct eastward dune propagation is seen in the Senkyo sand sea, and the orientations for Aztlan 552 kyr ago match observation, such that the dune orientations for all five sand seas can match observation for specific epochs and saltation threshold ranges. Agreement with the wind regime combining the four extrema of this cycle is also improved, with the correct orientations and eastward propagation being achieved in three (Fensal, Belet and Senkyo) rather than two dune fields, which was the case for the 45 kyr cycle.

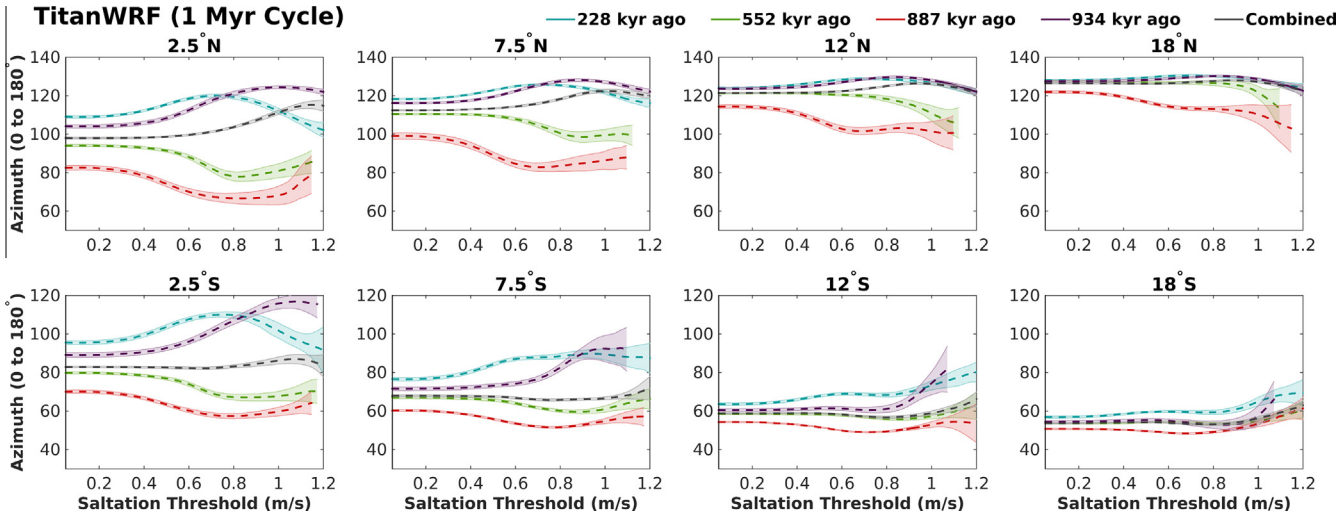

Fig. 7. Zonally averaged GBNT dune orientations predicted by the TitanWRF GCM without topography for the 1 Myr orbital cycle in L_s of perihelion at Saturn's maximum eccentricity. The plotting conventions are the same as those for Fig. 5.

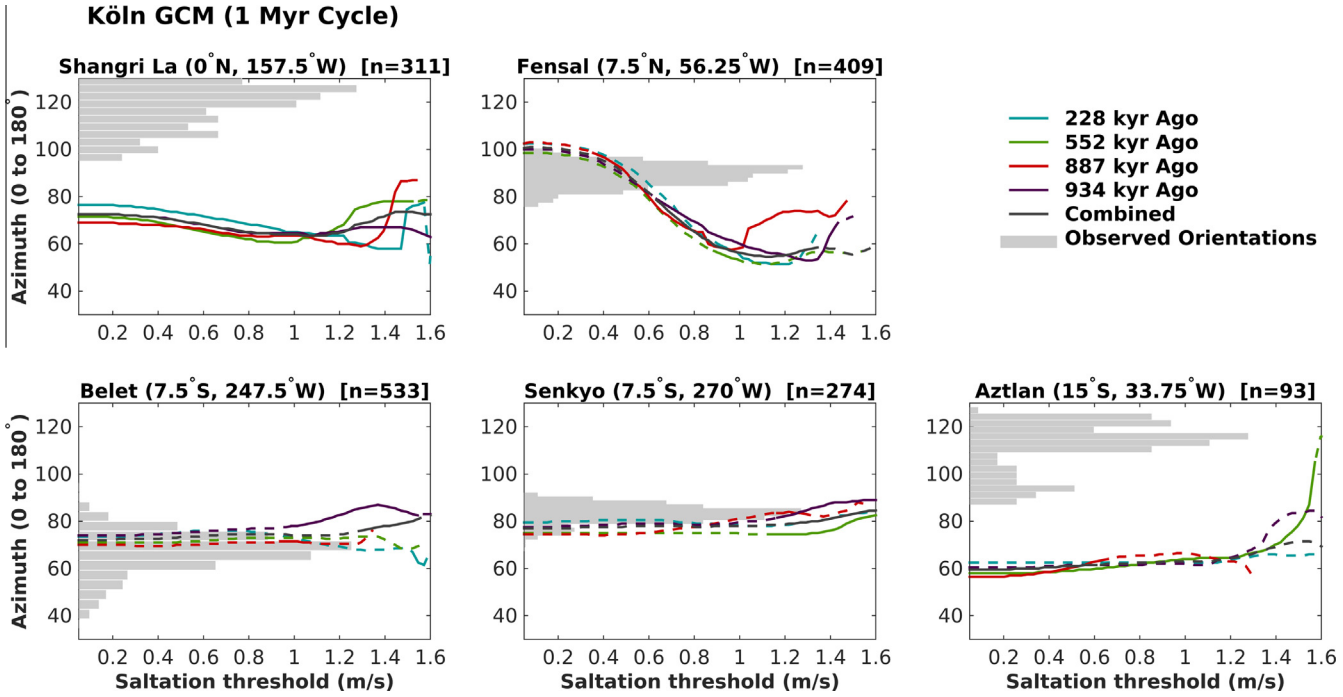

Fig. 8. GBNT dune orientations predicted by the Köln GCM with topography for the 1 Myr orbital cycle, at the locations of the five sand seas. The plotting conventions are the same as those of Fig. 6.

4. Conclusions

Using three different general circulation models, we have modeled Titan's climate under representative orbital configurations of its 45 kyr cycle in L_{sp} (solar longitude of perihelion), and the 1 Myr cycle in L_{sp} combined with Saturn's maximum eccentricity. Applying the GCM winds to a sediment transport model, we have predicted gross bedform-normal transport (GBNT) dune orientations across the equatorial region for each of the models.

Differences in the extent of the influence of orbital forcing on the dunes exist among the GCMs—with greater variations in the dune orientations predicted by TitanWRF and the Köln GCM (up to 50° and 70° respectively) as a function of epoch, when compared with TAM. Nevertheless, even in TAM, statistically significant differences in the dune orientations are seen for specific saltation thresholds and epochs. Thus, despite these differences, the consistent result across all tested GCMs is that the orbital configuration can affect the predicted dune orientations.

The relative importance of the 45 kyr and 1 Myr cycle in controlling the dune orientations depends on the reorientation timescale. In the first case, the reorientation timescales of the dunes is less than 45 kyr. In this case, the dunes will equilibrate to all or some combination of the orientations reported for the 4 extrema of the 45 kyr cycle. In the second scenario, the reorientation timescales of the dunes is greater than 45 kyr. In this case we expect the dunes to equilibrate with the orientations reported for each of the 4 orbital extrema in the 1 Myr cycle. Our simulations suggest somewhat improved agreement with observation for specific

epochs over others, but neither point to a single epoch that is in best agreement with observation or to particular epochs that can be ruled out. Based on these simulations, we cannot discount the possibility of a short reorientation timescale and the equilibration of the dunes to the modern wind regime, (although this would require higher sand fluxes that are not expected). However we suggest that based on the order 50,000 years reorientation timescale calculation laid out in Ewing et al. (2015) and Lorenz (2014), examination of the predicted orientations for longer reorientation timescales is important. Although other cycles exist in Titan's Croll–Milankovitch variations, we have focused on the L_{sp} and eccentricity variations that drive the largest changes in the solar insolation pattern at Titan (as discussed in Section 2.1). With the verification provided herein that the effect of orbital forcing can indeed be important in controlling dune orientations across multiple climate models, we emphasize that any study attempting to reconcile the modern-day orientations with a particular wind regime must consider the influence of orbital effects.

Our analysis shows that topography is important in producing the eastward dune propagation that is consistent with observation. Nevertheless, even for the model runs with topography, eastward propagation is found only in specific dune fields and for certain saltation thresholds. This finding may call into question the observational evidence for eastward propagation, and a re-examination of that evidence may prove fruitful. Alternatively, the inability of GCMs to capture regional events, such as methane storms, may preclude their ability to predict eastward propagation (Charnay et al., 2015).

We find situations where the modeled dune orientations closely match those that have been observed, and certain cases where the observed orientations are in better agreement with orientations modeled for previous epochs or the wind regime combining all four epochs over the current epoch (as discussed in 3.1.3). In particular, both the proper orientations and eastward crest propagation are found for the extremum of 33 kyr ago at multiple dune sites and in multiple GCMs. Nevertheless, there are many exceptions to this finding. Primarily westward dune propagation is seen in both TitanWRF and TAM, while there are disagreements between the modeled GBNT orientations and observed dune orientations for two of the five sand seas in both GCM runs with topography. Thus although no particular epoch exclusively matches the observed orientations, we have demonstrated that it is indeed possible to identify specific epochs or combinations of them that are in best agreement with observations.

Our analysis has focused on the effects that orbitally derived variations in the solar insolation have on the surface winds and in turn the dune orientations. There may be numerous secondary climatic changes resulting from orbital forcing that would affect the dunes. For example, on Earth, the extensive glaciation associated with the Last Glacial Maximum triggered dryer, stronger winds because of the enhanced thermal contrasts between low and mid-latitudes (Lautenschlager and Herterich, 1990). However, a decrease in the strength of tropical storms during the ice-age has also been suggested (Hobgood and Cerveny, 1988). Analogous effects of orbital forcing on the extent of Titan's surface liquid reservoirs have been shown to exist (Lora et al., 2014) and may also affect the methane storms—which should be explored in detail. We thus suggest that the variations in dune orientations among the orbital epochs presented herein may represent a minimum. Furthermore, GCM wind outputs are best interpreted as spatial averages over the grid size and thus underrepresent strong winds, suggesting that variability in the dune orientations among epochs at the regional scale will be even greater than for those shown here.

Matching in detail the observed orientations should be the focus of future work, for which consideration of dune orientations for the sediment availability-limited case may also prove fruitful. The discrepancies with observation that do exist in this work are expected given that no single Titan atmospheric model currently captures all effects responsible for the regional scale climate. E.g. high resolution surface boundary conditions (topography, albedo, etc.) are not yet available for most of Titan; and even with an active hydrological cycle, far higher spatial resolution than is typically used in a GCM would be needed to capture the detailed impact of a regional methane storm. Nevertheless, further study using model runs that produce these effects, in addition to higher spatial resolution and the possibility of runs lasting greater than one Titan year, may be useful in identifying a single epoch and that is in best agreement with observations.

Acknowledgments

We thank Paul Corlies for helpful suggestions in implementation of the sediment transport code, and Ralph Lorenz for suggesting use of the term Titan's Croll–Milankovitch cycles. We would also like to thank Sven Simon for useful feedback during the revision process. We thank the two anonymous reviewers for their constructive feedback. GDM, AGH, and RCE acknowledge support from NASA through the Cassini Data Analysis Program Grant NNX14AD52G. CEN acknowledges support from NASA OPR Grants NNX10AI26G and NNX11AM35G. All TitanWRF simulations were conducted on NASA's HEC Pleiades cluster. TT was supported by DFG Grant TO269/4-1. AL was supported by the Agence Nationale de la Recherche (ANR-12-BS0500103/EXO-DUNES). The user-made Matlab functions CircStat, WindRose, and shadedErrorBar were used extensively, and we thank the authors of these functions.

Appendix A. Supplementary material

The supplementary materials for this article include the Supplementary Information file, and the Matlab function `gbnt_rdd.m`, which was used to calculate the GBNT dune orientations and resultant drift directions presented in this paper. The Supplementary Information includes analyses demonstrating that wind outputs were sampled from the GCMs in sufficient numbers to calculate dune orientations, and documentation for using the provided `gbnt_rdd` function. The dune orientation data plotted in Figs. 5–8 will be made available on the corresponding author's website (http://www.prism.gatech.edu/~gmcdonald6), and the corresponding author welcomes inquiries concerning access to data.

Supplementary data associated with this article can be found, in the online version, at http://dx.doi.org/10.1016/j.icarus.2015.11.036.

References

Aharonson, O. et al., 2009. An asymmetric distribution of lakes on Titan as a possible consequence of orbital forcing. Nat. Geosci. 2 (12), 851–854. http://dx.doi.org/10.1038/ngeo698, ISSN 1752-0894.

Ayoub, F. et al., 2014. Threshold for sand mobility on Mars calibrated from seasonal variations of sand flux. Nat. Commun. 5, 1–8. http://dx.doi.org/10.1038/ncomms6096.

Barnes, J.W. et al., 2008. Spectroscopy, morphometry, and photoclinometry of Titan's dunefields from Cassini/VIMS. Icarus 195 (1), 400–414. http://dx.doi.org/10.1016/j.icarus.2007.12.006, ISSN 00191035.

Barnes, J.W. et al., 2012. AVIATR-Aerial Vehicle for In-situ and Airborne Titan Reconnaissance. Experimen. Astron. 33 (1), 55–127. http://dx.doi.org/10.1007/s10686-011-9275-9, ISSN 09226435.

Beveridge, C. et al., 2006. Development of spatially diverse and complex dune-field patterns: Gran Desierto Dune Field, Sonora, Mexico. Sedimentology 53 (6), 1391–1409. http://dx.doi.org/10.1111/j.1365-3091.2006.00814.x, ISSN 00370746.

Bird, M.K. et al., 2005. The vertical profile of winds on Titan. Nature 438 (7069), 800–802. http://dx.doi.org/10.1038/nature04060, ISSN 0028-0836.

Burr, D.M. et al., 2015. Higher-than-predicted saltation threshold wind speeds on Titan. Nature 517 (7532), 60–63. http://dx.doi.org/10.1038/nature14088, ISSN 0028-0836 <http://www.nature.com/doifinder/10.1038/nature14088>.
Charnay, B., Lebonnois, S., 2012. Two boundary layers in Titans lower troposphere inferred from a climate model. Nat. Geosci. 5 (2), 106–109. http://dx.doi.org/10.1038/ngeo1374, ISSN 1752-0894.
Charnay, B. et al., 2015. Methane storms as a driver of Titans dune orientation. Nat. Geosci. 8 (1), 362–366. http://dx.doi.org/10.1038/ngeo2406, ISSN 1752-0894.
Clark, R.N. et al., 2010. Detection and mapping of hydrocarbon deposits on Titan. J. Geophys. Res. E: Planets 115 (10), doi:http://dx.doi.org/10.1029/2009JE003369, ISSN 01480227.
Courrech du Pont, S. et al., 2014. Two modes for dune orientation. Geology, 743–747. http://dx.doi.org/10.1130/G35657.1, ISSN 0091-7613 <http://geology.gsapubs.org/cgi/doi/10.1130/G35657.1>.
Elachi, C. et al., 2005. Radar: The Cassini Titan RADAR mapper. Space Sci. Rev. 115 (1–4), 71–110. http://dx.doi.org/10.1007/s11214-004-1438-9, ISSN 00386308.
Ewing, R.C. et al., 2015. Sand dune patterns on Titan controlled by long-term climate cycles. Nat. Geosci. 8 (1), 15–19. http://dx.doi.org/10.1038/ngeo2323, ISSN 1752-0894 <http://www.nature.com/doifinder/10.1038/ngeo2323>.
Fryberger, S., Dean, G., 1979. A Study of Global Sand Seas. USGS.
Garratt, J.R., 1977. Review of drag coefficients over oceans and continents. Mon. Weath. Rev. 105 (7), 915–929. http://dx.doi.org/10.1175/1520-0493(1977)105<0915:RODCOO>2.0.CO;2, ISSN 0027-0644.
Gordon, C.T., Stern, W.F., 1982. A description of the GFDL global spectral model. Mon. Weath. Rev. 110 (7), 625–644. http://dx.doi.org/10.1175/1520-0493(1982)110<0625:ADOTGG>2.0.CO;2, ISSN 0027-0644.
Hobgood, J.S., Cerveny, R.S., 1988. Ice-age hurricanes and tropical storms. Nature 333, 243–245.
Hong, S.-Y., Pan, H.-L., 1996. Nonlocal boundary layer vertical diffusion in a medium-range forecast model. Mon. Weath. Rev. 124, 2322–2339.
Iess, L. et al., 2010. Gravity field, shape, and moment of inertia of Titan. Science (New York, NY) 327 (5971), 1367–1369. http://dx.doi.org/10.1126/science.1182583, ISSN 0036-8075.
Jennings, D.E. et al., 2011. Seasonal changes in Titan's surface temperatures. Astron. J. Lett. 737. http://dx.doi.org/10.1088/2041-8205/737/1/L15, ISSN 2041-8205 <http://hdl.handle.net/2060/20110008086> L15.
Karkoschka, E., 2016. Titans meridional wind profile and Huygens orientation and swing inferred from the geometry of DISR imaging. Icarus 270, 326–338.
Lancaster, N. et al., 2002. Late Pleistocene and Halocene dune activity and wind regimes in the western Sahara Desert of Mauritania. Geology 30 (11), 991–994. http://dx.doi.org/10.1130/0091-7613(2002)030<0991:LPAHDA>2.0.CO;2, ISSN 00917613.
Lautenschlager, M., Herterich, K., 1990. Atmospheric response to Ice Age conditions: Climatology near the Earth's surface. J. Geophys. Res. 95 (D13), 22547. http://dx.doi.org/10.1029/JD095iD13p22547, ISSN 0148-0227.
Le Gall, a. et al., 2011. Cassini SAR, radiometry, scatterometry and altimetry observations of Titan's dune fields. Icarus 213 (2), 608–624. http://dx.doi.org/10.1016/j.icarus.2011.03.026, ISSN 00191035.
Le Mouélic, S. et al., 2010. Global mapping of Titan in the infrared using a heuristic approach to reduce the atmospheric scattering component. In: 2nd Workshop on Hyperspectral Image and Signal Processing: Evolution in Remote Sensing, WHISPERS 2010 – Workshop Program, vol. 1(1), pp. 6–9, doi:http://dx.doi.org/10.1109/WHISPERS.2010.5594903.
Lebonnois, S. et al., 2014. Cambridge books online. In: Mueller-Wodarg, I., Griffith, C.A., Lellouch, E., Cravens, T.E. (Eds.), Titan: Surface, Atmosphere and Space Environment. Cambridge University Press, pp. 122–157, ISBN 9780511973420 (chap. 4).
Levison, H.F., Duncan, M.J., 1994. The long-term dynamical behavior of short-period comets. Icarus 108, 18–36. http://dx.doi.org/10.1006/icar.1994.1039, ISSN 0019-1035.
Lora, J.M., Mitchell, J.L., 2015. Titan's asymmetric lake distribution mediated by methane transport due to atmospheric eddies. Geophys. Res. Lett. 42 (1), 6213–6220. http://dx.doi.org/10.1002/2015GL064912.Abstract.
Lora, J.M. et al., 2014. Simulations of Titans paleoclimate. Icarus 243, 264–273. http://dx.doi.org/10.1016/j.icarus.2014.08.042, ISSN 00191035.
Lora, J.M. et al., 2015. GCM simulations of Titans middle and lower atmosphere and comparison to observations. Icarus 250, 516–528. http://dx.doi.org/10.1016/j.icarus.2014.12.030, ISSN 00191035.
Lorenz, R.D., 2008. A review of ballon concepts for Titan. J. Brit. Interplanet. Soc. 61 (1), 2–13.
Lorenz, R.D., 2014. Physics of saltation and sand transport on Titan: A brief review. Icarus 230, 162–167. http://dx.doi.org/10.1016/j.icarus.2013.06.023, ISSN 00191035.
Lorenz, R.D., Radebaugh, J., 2009. Global pattern of Titan's dunes: Radar survey from the Cassini prime mission. Geophys. Res. Lett. 36 (3), 11–14. http://dx.doi.org/10.1029/2008GL036850, ISSN 00948276.
Lorenz, R.D. et al., 2006. The sand seas of Titan: Cassini RADAR observations of longitudinal dunes. Science (New York, NY) 312 (5774), 724–727. http://dx.doi.org/10.1126/science.1123257, ISSN 0036-8075.
Lorenz, R.D. et al., 2010. A 3 km atmospheric boundary layer on Titan indicated by dune spacing and Huygens data. Icarus 205 (2), 719–721. http://dx.doi.org/10.1016/j.icarus.2009.08.002, ISSN 00191035.
Lorenz, R.D. et al., 2013. A global topographic map of Titan. Icarus 225 (1), 367–377. http://dx.doi.org/10.1016/j.icarus.2013.04.002, ISSN 00191035.
Lucas, A. et al., 2014. Growth mechanisms and dune orientation on Titan. Geophys. Res. Lett., 6093–6100 http://dx.doi.org/10.1002/2014GL060971, ISSN 00948276.
Lucas, A. et al., 2015. Sediment flux from the morphodynamics of elongating linear dunes. Geology 43 (11), 1027–1030.
Manabe, S. et al., 1965. Simulated climatology of a general circulation model with a hydrologic cycle. Mon. Weath. Rev. 93 (December), 769–798. http://dx.doi.org/10.1175/1520-0493(1965)093<0769:SCOAGC>2.3.CO;2, ISSN 0027-0644.
McKay, C.P. et al., 1989. The thermal structure of Titan's atmosphere. Icarus 80, 23–53. http://dx.doi.org/10.1016/0019-1035(89)90160-7, ISSN 00191035.
Mitchell, J.L. et al., 2006. The dynamics behind Titan's methane clouds. Proc. Nat. Acad. Sci. USA 103 (49), 18421–18426. http://dx.doi.org/10.1073/pnas.0605074103, ISSN 0027-8424.
Mitchell, J.L. et al., 2009. The impact of methane thermodynamics on seasonal convection and circulation in a model Titan atmosphere. Icarus 203 (1), 250–264. http://dx.doi.org/10.1016/j.icarus.2009.03.043, ISSN 00191035.
Neish, C.D., Lorenz, R.D., 2014. Elevation distribution of Titan's craters suggests extensive wetlands. Icarus 228, 27–34. http://dx.doi.org/10.1016/j.icarus.2013.09.024, ISSN 00191035.
Newman, C.E. et al., 2011. Stratospheric superrotation in the TitanWRF model. Icarus 213 (2), 636–654. http://dx.doi.org/10.1016/j.icarus.2011.03.025.
Ping, L. et al., 2014. Emergence of oblique dunes in a landscape-scale experiment. Nat. Geosci. 7 (2), 99–103. http://dx.doi.org/10.1038/ngeo2047, ISSN 1752-0894 <http://www.nature.com/doifinder/10.1038/ngeo2047>.
Radebaugh, J. et al., 2008. Dunes on Titan observed by Cassini Radar. Icarus 194 (2), 690–703. http://dx.doi.org/10.1016/j.icarus.2007.10.015, ISSN 00191035.
Radebaugh, J. et al., 2010. Linear dunes on Titan and Earth: Initial remote sensing comparisons. Geomorphology 121 (1–2), 122–132. http://dx.doi.org/10.1016/j.geomorph.2009.02.022, ISSN 0169555X.
Richardson, M.I. et al., 2007. PlanetWRF: A general purpose, local to global numerical model for planetary atmospheric and climate dynamics. J. Geophys. Res. E: Planets 112 (9), 1–29. http://dx.doi.org/10.1029/2006JE002825, ISSN 01480227.
Rodriguez, S. et al., 2014. Global mapping and characterization of Titan's dune fields with Cassini: Correlation between RADAR and VIMS observations. Icarus 230, 168–179. http://dx.doi.org/10.1016/j.icarus.2013.11.017, ISSN 00191035.
Rubin, D., Hunter, R., 1987. Bedform alignment in directionally varying flows. Science 237, 276–278.
Rubin, D., Ikeda, H., 1990. Flume experiments on the alignment of transverse, oblique, and longitudinal dunes in directionally varying flows. Sedimentology 37, 673–684.
Stiles, B.W. et al., 2008. Determining Titan's spin sate from Cassini RADAR images. Astron. J. 135 (5), 1669–1680. http://dx.doi.org/10.1088/0004-6256/135/5/1669, ISSN 0004-6256.
Suarez, M., Takacs, L., 1994. Documentation of the ARIES/GEOS dynamical core: Version 2. NASA Technical Memorandum 104606 5, 1–45.
Tokano, T., 2008. Dune-forming winds on Titan and the influence of topography. Icarus 194 (1), 243–262. http://dx.doi.org/10.1016/j.icarus.2007.10.007, ISSN 00191035.
Tokano, T., 2009. The dynamics of Titan's troposphere. Philos. Trans. Ser. A, Math., Phys., Eng. Sci. 367 (1889), 633–648. http://dx.doi.org/10.1098/rsta.2008.0163, ISSN 1364-503X.
Tokano, T., 2010. Relevance of fast westerlies at equinox for the eastward elongation of Titan's dunes. Aeol. Res. 2 (2–3), 113–127. http://dx.doi.org/10.1016/j.aeolia.2010.04.003, ISSN 18759637.
Tokano, T. et al., 1999. Seasonal variation of Titan's atmospheric structure simulated by a general circulation model. Planet. Space Sci. 47 (3–4), 493–520, ISSN 00320633.
Tokano, T. et al., 2006. Titan's planetary boundary layer structure at the Huygens landing site. J. Geophys. Res. 111 (E8), 1–10. http://dx.doi.org/10.1029/2006JE002704, ISSN 0148-0227.
von Kármán, T., 1930. Mechanische Ähnlichkeit und Turbulenz. Nachrichten von der Gesellschaft der Wissenschaften zu Göttingen – Fachgruppe I (Mathematik) 5, 58–76.
Ward, W.R., Hamilton, D.P., 2004. Tilting Saturn. I. Analytic model. Astron. J. 128 (5), 2501–2509. http://dx.doi.org/10.1086/424533, ISSN 0004-6256.
White, B.R., 1979. Soil transport by winds on Mars. J. Geophys. 84, 4463–4651. http://dx.doi.org/10.1029/JB084iB09p04643, ISSN 0148-0227.
Zebker, H.a. et al., 2009. Size and shape of Saturn's Moon Titan. Science (New York, NY) 324 (5929), 921–923. http://dx.doi.org/10.1126/science.1168905, ISSN 0036-8075.